Paleoceanography

Supporting Information for

Deglacial subarctic Pacific surface water hydrography and nutrient dynamics and links to North Atlantic climate variability and atmospheric CO_2

E. Maier[1#], M. Méheust[1], A. Abelmann[1], R. Gersonde[1], B. Chapligin[2], J. Ren[1], R. Stein[1], H. Meyer[2], R. Tiedemann[1]

[1]Alfred Wegener Institute Helmholtz Centre for Polar and Marine Research, 27568 Bremerhaven, Germany
[2]Alfred Wegener Institute Helmholtz Centre for Polar and Marine Research, 14473 Potsdam, Germany

[#]corresponding author: Edith Maier, Alfred Wegener Institute, Helmholtz Centre for Polar and Marine Research, Am Alten Hafen 26, 27570 Bremerhaven (edith.maier@awi.de)

Contents of this file

Introduction

Figure S1 demonstrates the effectivity of sonication for the purification of diatom samples for isotope analyses, since sonication helps separating diatoms from other biogenic silicates (radiolarians, sponge spicules).

Figure S2 describes in detail the error estimation of the local surface seawater oxygen isotope composition.

Figure S3 shows the diatom isotopic data on different time scales to test the robustness of the main scientific findings.

Figure S4 shows the residual contamination of the purified SO202-27-6 diatom samples with non-biogenic silicates (determined by Energy Dispersive X-ray spectrometry (EDS) and Inductively Coupled Plasma Optical Emission Spectrometry (ICP-OES); details are given in the main text, section 3.2). Mass-balance corrections of the diatom oxygen and silicon isotope records show that even assuming extreme theoretical oxygen and silicon isotope values for the contamination the general features of the diatom isotope records are not level out (details on mass-balance corrections are given in the main text, section 3.2).

Figure S5 presents the relative diatom abundances in the pre-sonicated diatom samples and the Si utilization calculated from the SO202-27-6 $\delta^{30}Si_{diat}$ values using three different fractionation factors for *C. marginatus* and *C. oculus-iridis*.

Table S1 presents all main information regarding the age models of cores MD01-2416 and MD02-2489, for which partly new age control points were determined (for details see main text, section 4).

Table S2 shows the percentages of SiO_2 and Al_2O_3 within the purified diatom samples from cores SO202-27-6 and MD01-2416, determined/estimated by EDS/ICP-OES, as well as inferred percentages of contamination with non-biogenic silicates (e.g. rock fragments, clay minerals) (details are given in the main text, section 3.2)

Table S3 presents the compositions of the pre-sonicated diatom samples, determined by light microscopy, and of the final purified diatom samples, determined by Scanning Electron Microscopy (details on the counting procedures are found in the main text, section 3.2).

Table S4 shows the diatom oxygen and silicon isotope values of cores SO202-27-6 and MD01-2416, as well as standard deviations and number of isotopic measurements. Isotope analyses were carried out according to the procedures described by *Maier et al.* [2013] and *Chapligin et al.* [2010].

Table S5 presents the results of oxygen and carbon isotope analyses on planktic foraminifer *N. pachyderma*$_{sin}$, as well as the biogenic opal content, opal mass accumulation rates and X-ray fluorescence intensities from Core SO202-27-6 (details on procedures are given in the main text, section 3)

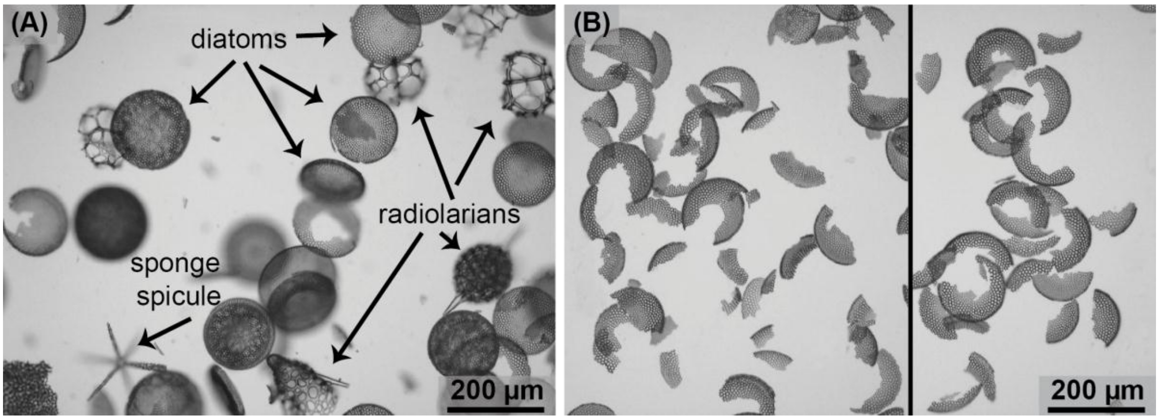

Figure S1. SO202-27-6 diatom sample from core depth 77-79 cm in two steps of purification process (pictures were taken using a ProgRes C10 plus digitale camera coupled to a Zeiss Axioplan II light microscope. (A) Diatom sample after heavy liquid separation and prior to sonication. (B) Final purified diatom sample.

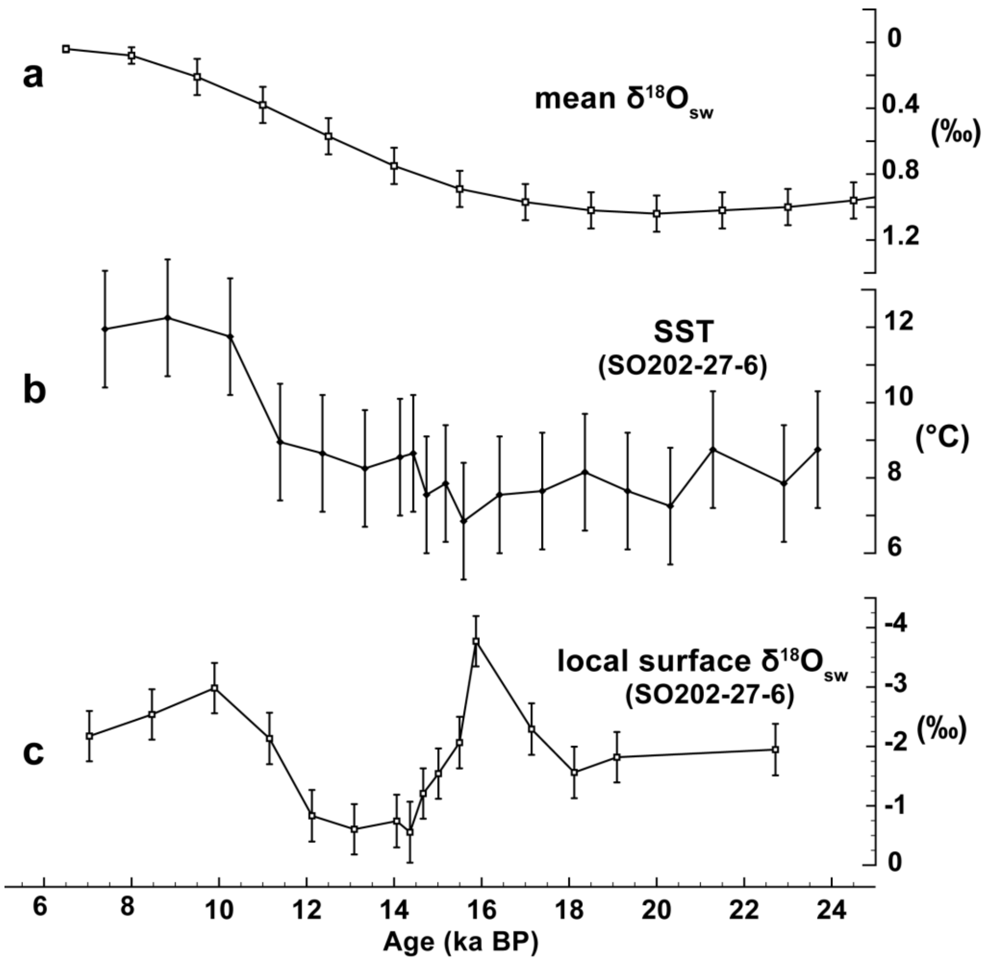

Figure S2. (a) Global mean seawater $\delta^{18}O$ ($\delta^{18}O_{sw}$) and errors [from *Waelbroeck et al.*, 2002]; **(b)** alkenone-based SST record including error bars (=1.55°C) from Core SO202-27-6. **(c)** Local surface $\delta^{18}O_{sw}$ record calculated according to the following equation based on *Juillet-Leclerc and Labeyrie* [1987]:

$$\textbf{local surface } \boldsymbol{\delta^{18}O_{sw}} = \boldsymbol{\delta^{18}O_{diat}} - \mathbf{34} - \sqrt{\mathbf{122 - 5SST}} - \textbf{mean } \boldsymbol{\delta^{18}O_{sw}}$$

where $\delta^{18}O_{diat}$ is the measured diatom $\delta^{18}O$, SST is the temperature calculated from the alkenone-based SST record from the same core and mean $\delta^{18}O_{sw}$ is the mean seawater $\delta^{18}O$ [from *Waelbroeck et al.*, 2002]. To get SST and mean $\delta^{18}O_{sw}$ for the time points of the $\delta^{18}O_{diat}$ measurements, we did a linear interpolation of both data sets. The errors in local surface $\delta^{18}O_{sw}$ were estimated by propagating the error introduced by the $\delta^{18}O_{diat}$ measurement and the alkenone measurement (0.4°C), the alkenone:temperature calibration (1.5°C) and the removal of global ice volume [from *Waelbroeck et al.*, 2002]. We used the following equation to propagate the error, assuming no covariance among the errors [*Bevington and Robinson*, 2003: p. 41]:

$$\boldsymbol{\sigma^2_{local\,surface\,\delta^{18}O_{sw}} = \sigma^2_{\delta^{18}O_{diat}} + \sigma^2_{mean\,\delta^{18}O_{sw}} + \sigma^2_{SST} f'(SST)^2}$$

where

$$\boldsymbol{\sigma^2_{SST} = (0.4)^2 + (1.5)^2 = 2.41(^\circ C)^2}$$

$$\boldsymbol{f'(SST) = \frac{-5}{2\sqrt{122 - 5SST}}}$$

and $\sigma^2_{\delta^{18}O_{diat}}$ and $\sigma^2_{mean\ \delta^{18}O_{sw}}$ are the errors of the $\delta^{18}O_{diat}$ measurements and of the mean $\delta^{18}O_{sw}$, respectively.

Taking interpolation of SST and mean $\delta^{18}O_{sw}$ data into account, the variances of local surface $\delta^{18}O_{sw}$ were estimated as follows:

$$\sigma^2_{local\ surface\ \delta^{18}O_{sw}}(t_0) = \sigma^2_{\delta^{18}O_{diat}}(t_0) + \left(\frac{t_0 - t_1}{t_2 - t_1}\right)^2 \sigma^2_{mean\ \delta^{18}O_{sw}}(t_2)$$

$$+ \left(1 - \frac{t_0 - t_1}{t_2 - t_1}\right)^2 \sigma^2_{mean\ \delta^{18}O_{sw}}(t_1)$$

$$+ \frac{25\sigma^2_{SST}}{488 - 20(\frac{t_0 - t_3}{t_4 - t_3} SST(t_4) + (1 - \frac{t_0 - t_3}{t_4 - t_3} SST(t_3))}$$

where

$\sigma^2_{local\ surface\ \delta^{18}O_{sw}}(t_0)$ is the variance of local surface $\delta^{18}O_{sw}$ at the time t_0, which corresponds to the time of the $\delta^{18}O_{diat}$ measurement,

$\sigma^2_{\delta^{18}O_{diat}}(t_0)$ is the variance of the $\delta^{18}O_{diat}$ measurement at the time t_0,

t_1 and t_2 are the time points of the mean $\delta^{18}O_{sw}$ data closest to t_0, where $t_1 \leq t_0 \leq t_2$,

$\sigma^2_{mean\ \delta^{18}O_{sw}}(t_1)$ and $\sigma^2_{mean\ \delta^{18}O_{sw}}(t_2)$ are the variances of the mean $\delta^{18}O_{sw}$ data at the time t_1 and t_2, respectively,

$\sigma^2_{SST} = 2.41$,

t_3 and t_4 are the time points of the SST data closest to t_0, where $t_3 \leq t_0 \leq t_4$

and

$SST(t3)$ and $SST(t4)$ are the SST values at the time t_3 and t_4, respectively.

The resulting error for local surface $\delta^{18}O_{sw}$ is 0.44 ± 0.02‰.

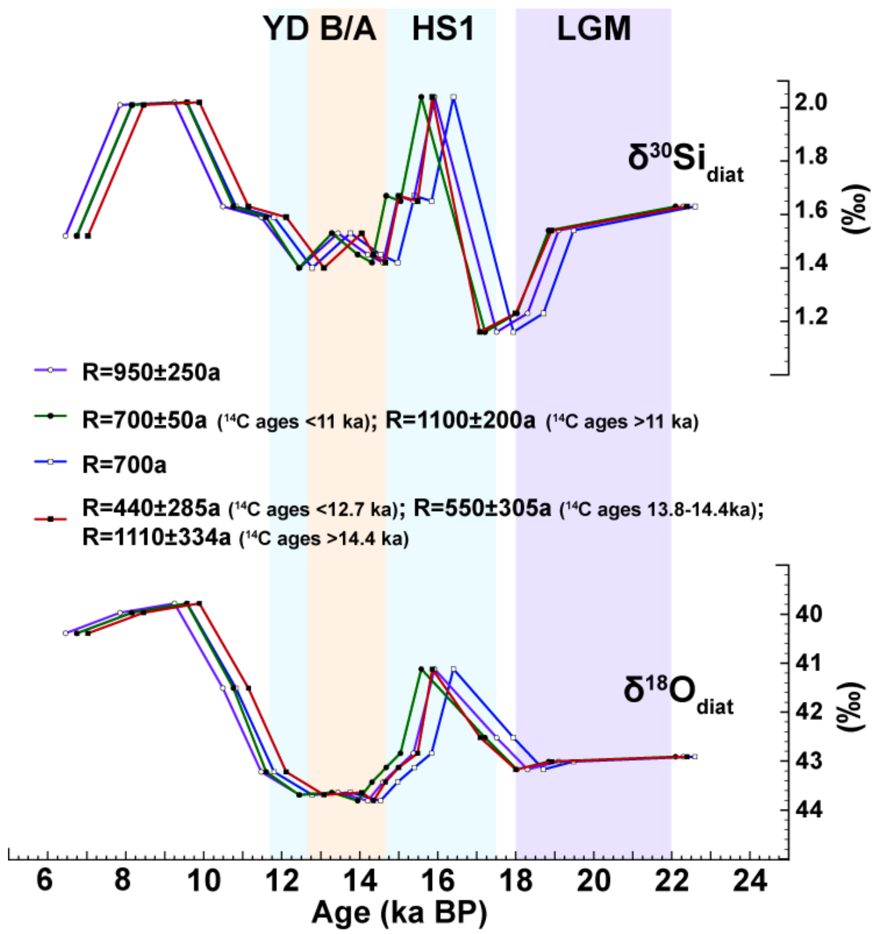

Figure S3. SO202-27-6 $\delta^{30}Si_{diat}$ and $\delta^{18}O_{diat}$ records plotted on different time scales to test the robustness of our main findings. The SO202-27-6 age models were constructed based on planktic ^{14}C ages, using different planktic reservoir ages and different age model construction techniques previously applied on deglacial sequences of subarctic Pacific sediment cores: Three age models were constructed solely by calibrating the six raw planktic ^{14}C ages of SO202-27-6 using the Calib 7.1 software and the Marine09 calibration dataset [*Stuiver and Reimer*, 1993; *Reimer et al.*, 2013], however applying different reservoir ages: (1) 700 years over the whole core section (blue line, white circles). A constant reservoir age of about 700 has previously been applied on sediment cores from the NW [*Keigwin*, 1987; *Keigwin et al.*, 1992; *Sabin and Pisias*, 1996] and NE Pacific [*Lopes and Mix*, 2009; *Lund et al.*, 2011]; (2) 950±250 years over the whole core section, as used by *Galbraith et al.* [2007] for core ODP 887 located close to Core SO202-27-6 (purple line, white diamonds); (3) 700±50 years for ^{14}C ages <11 ka and 1100±200 years for ^{14}C ages >11ka, based on *Kienast and McKay* [2001] and *Kovanen and Easterbrook* [2002] for the NE Pacific (green line, black circles). The fourth age model of SO202-27-6, which we apply in this study, was constructed using a combination of calibrated ^{14}C ages and correlation to the well-dated Core MD02-2489, located close to Core SO202-27-6 (red line, black squares) (Figure 2; section 4).

It is important to note that the main changes of the isotopic signals discussed in the main text, particularly the low $\delta^{30}Si_{diat}$ at the start of the deglaciation, the high $\delta^{30}Si_{diat}$/low $\delta^{18}O_{diat}$ during mid-HS1 and the intermediate $\delta^{30}Si_{diat}$/high $\delta^{18}O_{diat}$ during the B/A, occur within the same time intervals independent from the choice of the age model, highlighting the robustness of our findings.

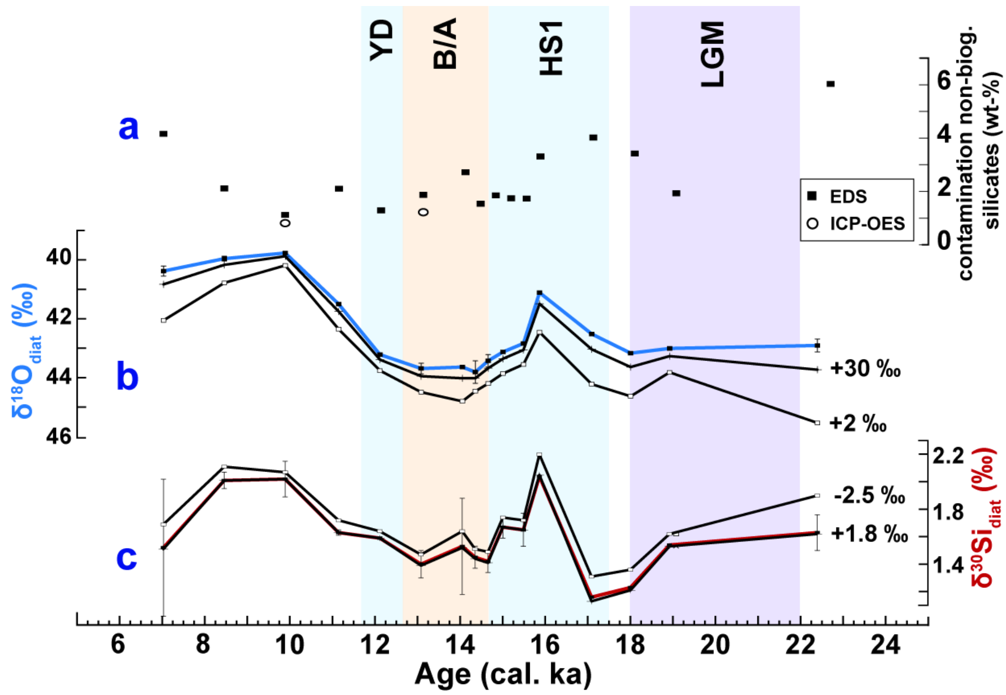

Figure S4. (a) Contamination of purified SO202-27-6 diatom samples with non-biogenic silicates estimated by inductively coupled plasma optical emission spectrometry (ICP-OES) and energy dispersive X-ray spectrometry (EDS). **(b)** and **(c)** Measured SO202-27-6 $\delta^{18}O_{diat}$ (b; blue curve) and $\delta^{30}Si_{diat}$ (c; red curve) records including isotopic curves mass-balance corrected for contamination with non-biogenic silicates estimated by EDS and using two different theoretical $\delta^{18}O_{cont}$ (+2‰ and +30‰) and $\delta^{30}Si_{cont}$ (-2.5‰ and +1.8‰) values (black curves). Error bars indicate errors (1σ) of replicate analyses.

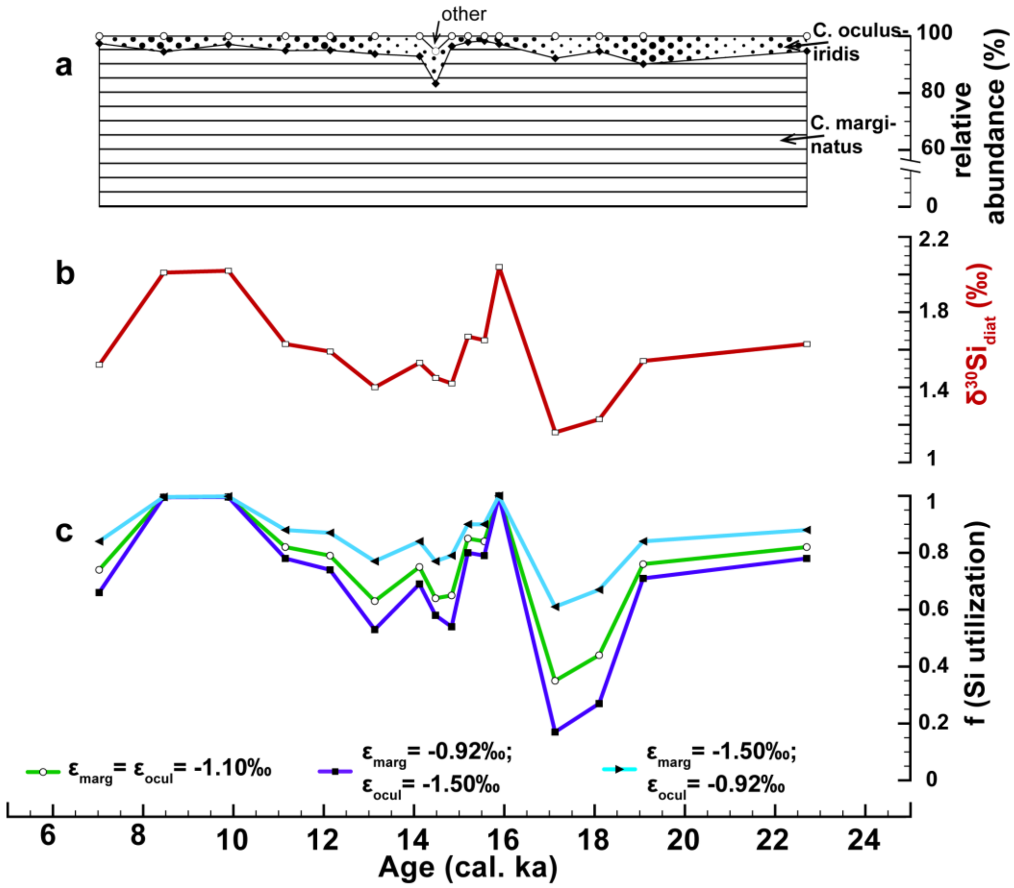

Figure S5. (a) Relative diatom abundances in the pre-sonicated SO202-27-6 diatom samples. Only one sample contains diatoms other than from the genus *Coscinodiscus*. **(b)** Measured SO202-27-6 $\delta^{30}Si_{diat}$ record. **(c)** Si utilization calculated from the SO202-27-6 $\delta^{30}Si_{diat}$ values, assuming a closed system with a Rayleigh –type fractionation according to the following equation:

$$\delta^{30}Si_{diat} = \delta^{30}Si_{isw} - \left(\frac{1-f}{f}\right)\varepsilon \ln(1-f)$$

where $\delta^{30}Si_{isw}$ is the δ^{30}Si value of the silicic acid of the initial source seawater, *f* is the degree of Si utilization and ε is the fractionation factor. Since there is yet no information on silicic acid δ^{30}Si from the open ocean NE Pacific water column, we used a $\delta^{30}Si_{isw}$ value of +2.04‰ for our calculations, which corresponds to the highest $\delta^{30}Si_{diat}$ measured in Core SO202-27-6. We applied 3 different fractionation factors (ε) for *C. marginatus* and *C. oculus-iridis* to test the influence of potentially different ε on the Si utilization pattern and on absolute values of Si utilization. An ε of -1.1‰ corresponds to the average ε determined by *De la Rocha et al.* [1997] and *Milligan et al.* [2004] for diatom species from the genus *Thalassiosira*, which belong to the same diatom suborder as the genus *Coscinodiscus* . We furthermore calculated Si utilization using a ε of -0.92‰ for *C. marginatus* and an ε of -1.50‰ for *C. oculus-iridis*, and vice versa; These are the endmember ε determined in culture studies of *Thalassiosira* species [*Sutton et al., 2013*; *Sun et al., 2014*]. While the application of different ε does not change the relative pattern of Si utilization, absolute changes and values of Si utilization strongly depend on the applied ε.

Table S1. Age control points of cores **(A)** MD01-2416 and **(B)** MD02-2489. Planktic (*N. pachyderma$_{sin}$*) radiocarbon ages of **(A)** Core MD01-2416 [*Sarnthein et al.*, 2004; 2007], and **(B)** Core MD02-2489 [*Gebhardt et al.*, 2008], including newly calibrated ages. Reservoir ages and ^{14}C-plateau boundaries were taken from *Sarnthein et al.* [2015]. **(A)** The depth of the ^{14}C-plateau IIa base/IIb top within Core MD01-2416, not provided by *Sarnthein et al.* [2015], was determined assuming a constant sedimentation rate over ^{14}C-plateau II (depth marked by an *). **(B)** Since the ^{14}C record of Core MD02-2489 does no reach as far back as to allow for the determination of the base of ^{14}C-plateau Va [see *Sarnthein et al*., 2015], the age model prior to 19.130 ka BP (top of ^{14}C-plateau Va) was constructed based on calibration of the ^{14}C value at 520 cm depth, using Calib 7.1, the Marine13 data set and a reservoir age of 1560±310 a (determined for ^{14}C-plateau Va by *Sarnthein et al.* [2015]), and linear interpolation in between.

(A) MD01-2416

Depth (cm) MD01-2416	^{14}C ages (ka) (Sarnthein et al.,2004; 2007)	^{14}C age error (a) (Sarnthein et al., 2004; 2007)	Reservoir age (a) (Sarnthein et al., 2015)	Calibrated ages (ka BP)	Derivation of cal. age (^{14}C-plateau boundaries after *Sarnthein et al.* (2015)	Calib 7.1 calibrated ages (ka BP) Median (ka BP)	2σ min (ka BP)	2σ max (ka BP)	Relative area under probability distribution
0.75	5.684	30	570 ± 138	**5.900**	Calib 7.1	5.900	5.593	6.205	1
16	6.745	33	570 ± 138	**7.077**	Calib 7.1	7.077	6.754	7.383	1
39	7.869	36	570 ± 138	**8.161**	Calib 7.1	8.161	7.867	8.431	1
51	9.985	35	570 ± 138	**10.754**	Calib 7.1	10.754	10.402	11.125	1
88	12.690	50	570 ± 138	**13.640**	Plateau Ia top	-	-	-	-
98	-	-	570 ± 138	**13.940**	Plateau Ia base	-	-	-	-
104	13.140	60	723 ± 284	**14.050**	Plateau I top	-	-	-	-
136	13.090	60	723 ± 284	**14.920**	Plateau I base	-	-	-	-
140.5	13.795	60	431 ± 253	**15.250**	Plateau IIa top	-	-	-	-
164.5*	-	-	431 ± 253 /1140 ± 199	**16.050**	P IIa base/ PIIb top*	-	-	-	-
175	-	-	1140 ± 199	**16.400**	Plateau IIb base	-	-	-	-
179	16.100	100	1479 ± 135	**16.900**	Plateau III top	-	-	-	-
199	16.230	199	1479 ± 135	**17.580**	Plateau III base	-	-	-	-

Table S1. (continued).

(B) MD02-2489

Depth (cm) MD02-2489	^{14}C ages (ka) (Gebhardt et al., 2008)	^{14}C age error (a) (Gebhardt et al., 2008)	Reservoir age (a) (Sarnthein et al., 2015)	Calibrated ages (ka BP)	Derivation of cal. age (^{14}C-plateau boundaries after Sarnthein et al. (2015)	Calib 7.1 calibrated ages (ka BP): Median (ka BP)	2σ min (ka BP)	2σ max (ka BP)	Relative area under probability distribution
59.0	7.570	40	440 ± 285	**8.003**	Calib 7.1	8.003	7.434	8.579	1
66.5	8.715	45	440 ± 285	**9.310**	Calib 7.1	9.310	8.587	10.092	1
76.5	9.210	50	440 ± 285	**9.933**	Calib 7.1	9.933	9.247	10.660	1
86.5	10.140	70	440 ± 285	**11.135**	Calib 7.1	11.135	10.327	12.070	1
96.0	11.080	60	440 ± 285	**12.445**	Calib 7.1	12.445	11.540	13.143	0.997
110.0	11.870	30	440 ± 285	**13.297**	Calib 7.1	13.297	12.714	13.873	1
119.0	12.120	70	440 ± 285	**13.567**	Calib 7.1	13.567	12.862	14.249	1
130.0	12.730	35	440 ± 285	**14.050**	Plateau I top	-	-	-	-
165.5	12.800	90	440 ± 285	**14.920**	Plateau I base	-	-	-	-
171.5	13.820	80	550 ± 305	**15.250**	Plateau IIa top	-	-	-	-
189.5	14.180	80	550 ± 305/120	**16.050**	P IIa base / P IIb top	-	-	-	-
200.5	14.430	90	550 ± 120	**16.400**	Plateau IIb base	-	-	-	-
208	-	-	805 ± 155	**16.900**	Plateau III top	-	-	-	-
219	-	-	805 ± 155	**17.300**	Plateau III base	-	-	-	-
231.0	16.750	110/100	1110 ± 334	**18.000**	Plateau IV top	-	-	-	-
260	-	-	1110 ± 334	**18.980**	Plateau IV base	-	-	-	-
268.0	18.042	65	1560 ± 310	**19.130**	Plateau Va top	20.427	19.583	21.312	1
520.0	30.521	170	1560 ± 310	**31.131**	Calib 7.1	31.131	30.034	31.883	1

Table S2. Contamination of purified diatom samples with non-biogenic silicates estimated from SiO_2 and Al_2O_3 percentages determined **(A)** by ICP-OES for Core SO202-27-6 and **(B, C)** by EDS for cores (B) SO202-27-6 and (C) MD01-2416.

(A)

		ICP-OES		
SO202-27-6 Depth (cm)	**Age (ka BP)**	**SiO_2 assumed (%)**	**Al_2O_3 (%)**	**non-biogenic silicate contamination (%)**
9-11	9.888	99.51	0.15	0.81
21-23	13.134	99.09	0.14	1.22

(B)

		EDS		
SO202-27-6 Depth (cm)	**Age (ka BP)**	**SiO_2 (%)**	**Al_2O_3 (%)**	**non-biogenic silicate contamination (%)**
1-3	7.029	98.1	1.0	4.2
5-6	8.458	98.9	0.5	2.1
9-11	9.888	99.3	0.2	1.1
13-15	11.144	98.9	0.4	2.1
17-19	12.113	99.1	0.2	1.3
21-23	13.081	98.8	0.3	1.9
25-27	14.050	98.2	0.4	2.7
29-31	14.353	98.8	0.2	1.5
33-35	*14.655*	98.7	0.2	1.8
37-39	15.003	98.8	0.3	1.7
41-43	15.485	98.9	0.3	1.7
45-47	15.862	97.9	0.6	3.3
53-55	17.087	97.7	0.8	4.0
57-59	18.002	98.0	0.7	3.4
61-63	18.918	98.6	0.3	1.9
77-79	22.391	96.9	1.4	6.0
Avg		98.5	0.5	2.6
SD (1σ)		0.6	0.3	1.3

(C)

		EDS		
MD01-2416 Depth (cm)	**Age (ka BP)**	**SiO_2 (%)**	**Al_2O_3 (%)**	**non-biogenic silicate contamination (%)**
4-8*	6.292	99.17	0.10	1.1
12-16*	6.920	99.18	0.12	1.1
22-26*	7.454	99.07	0.18	1.3
32-36*	7.925	99.14	0.07	1.0
38-40	8.161	98.82	0.24	1.7
42-46	9.241	99.13	0.12	1.1
48-50	10.322	99.05	0.12	1.2
52-56*	10.995	99.08	0.11	1.2
62-66*	11.796	99.07	0.12	1.2
68-70	12.197	99.05	0.11	1.2
72-76*	12.638	99.13	0.10	1.1
78-80	12.999	98.86	0.14	1.4
82-86*	13.400	98.94	0.12	1.3
92-96*	13.849	99.03	0.11	1.2
102-106	14.125	98.98	0.09	1.2
Avg		99.0	0.1	1.2
SD (1σ)		0.1	0.0	0.2

*data from *Maier et al.* [2013]

Table S3. Composition of **(A)** pre-sonicated and **(B)** final purified SO202-27-6 diatom samples. **(A)** Relative abundances of diatoms, radiolarians and sponge spicules are related to the total counts and relative abundances of *Coscinodiscus marginatus* and *Coscinodiscus oculus-iridis* are related to the diatom species assemblage, determined by light microscopy. Note that the sample 29-31 cm is the only sample were non-*Coscinodiscus* diatoms contribute to the diatom species assemblage (5.3%). **(B)** All relative abundances, determined under the Scanning Electron Microcope (SEM), are related to the total counts.

(A)

		light microscopy (pre-sonication)					
SO202-27-6 Depth (cm)	**Age (ka BP)**	**total counts**	**diatoms (%)**	**radiolarians (%)**	**sponge spicules (%)**	***C. marginatus* (% of diatom abundance)**	***C. oculus-iridis* (% of diatom abundance)**
1-3	7.029	201	96.5	3.5	0.0	97.4	2.6
5-6	8.458	216	84.3	15.3	0.5	94.5	5.5
9-11	9.888	159	88.1	10.7	1.3	97.1	2.9
13-15	11.144	221	62.4	34.4	3.2	94.9	5.1
17-19	12.113	158	88.6	11.4	0.0	95.0	5.0
21-23	13.081	215	88.8	9.8	1.4	93.7	6.3
25-27	14.050	123	91.1	8.9	0.0	92.9	7.1
29-31	14.353	169	88.8	11.2	0.0	83.3	11.3
33-35	*14.655*	213	92.5	7.0	0.5	96.4	3.6
37-39	15.003	154	92.2	7.1	0.6	97.9	2.1
41-43	15.485	139	84.2	13.7	2.2	98.3	1.7
45-47	15.862	189	76.2	23.3	0.5	97.2	2.8
53-55	17.087	217	53.5	46.5	0.0	92.2	7.8
57-59	18.002	354	36.4	62.1	1.4	94.6	5.4
61-63	18.918	233	70.0	29.2	0.9	90.2	9.8
77-79	22.391	224	84.8	14.3	0.9	94.7	5.3
Avg		199	79.9	19.3	0.8	94.4	5.3
SD (1σ)		54	16.5	16.2	0.9	3.7	2.7

(B)

		SEM (purified)					
SO202-27-6 Depth (cm)	**Age (ka BP)**	**total counts**	**diatoms (%)**	**radiolarians (%)**	**sponge spicules (%)**	**non-biogenic silicate contamination (%)**	**not identified (%)**
1-3	7.029	423	96.5	3.3	0	0.2	0
5-6	8.458	391	96.4	3.1	0	0.3	0.3
9-11	9.888	496	97.8	1.6	0.2	0.4	0
13-15	11.144	394	97.5	0.5	1.0	1.0	0
17-19	12.113	509	97.2	2.6	0	0.2	0
21-23	13.081	337	91.4	8.0	0	0.6	0
25-27	14.050	249	96.4	3.2	0	0.4	0
29-31	14.353	289	88.2	10.0	0.7	0.3	0.7
33-35	*14.655*	242	95.9	3.3	0	0.8	0
37-39	15.003	344	90.7	6.1	0	3.2	0
41-43	15.485	322	99.1	0.6	0	0.3	0
45-47	15.862	326	92.0	6.7	0.6	0.6	0
53-55	17.087	269	91.8	5.2	0	2.6	0.4
57-59	18.002	281	91.8	6.8	0	1.4	0
61-63	18.918	349	90.0	9.2	0	0.6	0.3
77-79	22.391	233	95.7	3.9	0	0.4	0
Avg		341	94.3	4.6	0.2	0.8	0.1
SD (1σ)		84	3.3	2.9	0.3	0.9	0.2

Table S4. Measured $\delta^{18}O_{diat}$ and $\delta^{30}Si_{diat}$ values of Cores **(A)** SO202-27-6 and **(B)** MD01-2416 including standard deviations (SD, 1σ) and number of isotopic measurements (n).

(A)

SO202-27-6							
Depth (cm)	**Age (ka BP)**	**$\delta^{30}Si_{diat}$ (‰)**	**SD $\delta^{30}Si_{diat}$ (1σ; ‰)**	**n**	**$\delta^{18}O_{diat}$ (‰)**	**SD $\delta^{18}O_{diat}$ (1σ; ‰)**	**n**
1-3	7.029	1.52	0.50	3	40.39	0.17	3
5-7	8.458	2.01	0.06	2	39.97	0.08	2
9-11	9.888	2.02	0.13	3	39.78	0.05	2
13-15	11.144	1.63	0.02	2	41.51	0.03	2
17-19	12.113	1.59	0.01	2	43.22	0.06	2
21-23	13.081	1.40	0.10	2	43.69	0.18	3
25-27	14.050	1.53	0.35	3	43.64	0.04	3
29-31	14.353	1.45	0.08	3	43.81	0.38	3
33-35	*14.655*	1.42	0.08	2	43.43	0.21	2
37-39	15.003	1.67	0.08	2	43.13	0.06	3
41-43	15.485	1.65	0.12	3	42.84	0.04	2
45-47	15.862	2.04	-	1	41.12	-	1
53-55	17.087	1.16	-	1	42.52	-	1
57-59	18.002	1.23	-	1	43.17	-	1
61-63	18.918	1.54	-	1	43.01	-	1
77-79	22.391	1.63	0.13	2	42.91	0.22	2

(B)

MD01-2416							
Depth (cm)	**Age (ka BP)**	**$\delta^{30}Si_{diat}$ (‰)**	**SD $\delta^{30}Si_{diat}$ (1σ; ‰)**	**n**	**$\delta^{18}O_{diat}$ (‰)**	**SD $\delta^{18}O_{diat}$ (1σ; ‰)**	**n**
4-8*	6.292	1.19	0.01	2	42.31	0.29	2
12-16*	6.920	1.37	0.11	4	42.48	0.10	3
22-26*	7.454	1.31	0.06	2	42.57	0.20	2
32-36*	7.925	1.30	0.04	2	42.60	0.09	2
38-40	8.161	1.35	0.15	2	42.76	0.05	2
42-46	9.241	1.38	0.14	3	42.64	0.13	4
48-50	10.322	1.22	-	1	43.21	-	1
52-56*	10.995	1.30	0.04	3	43.10	0.08	2
62-66*	11.796	1.38	0.01	2	43.10	0.04	2
68-70	12.197	1.54	0.52	2	43.88	0.25	2
72-76*	12.638	1.46	0.01	3	43.68	0.13	2
78-80	12.999	1.10	-	1	43.99	-	1
82-86*	13.400	1.32	0.02	5	43.70	0.07	3
92-96*	13.849	1.34	0.01	2	43.64	0.05	2
102-106	14.125	1.29	0.02	3	43.84	0.35	3

*isotope data from *Maier et al.* [2013]

Table S5. Proxy data of Core SO202-27-6. **(A)** $\delta^{18}O_{Nps}$ and $\delta^{13}C_{Nps}$ values; **(B)** biogenic opal content; **(C)** opal mass accumulation rates; **(D)** XRF intensities (Fe, Ca and Si/Ti ratios).

(A)

Depth (cm)	Age (ka BP)	$\delta^{18}O$ (‰) *Nps*	$\delta^{13}C$ (‰) *Nps*	Size fraction (µm)
0-1	6.493	2.385	0.598	125-250
4-5	7.922	2.582	0.466	125-250
8-9	9.352	2.603	0.580	125-250
12-13	10.781	2.553	0.417	125-250
16-17	11.750	2.873	0.407	125-250
20-21	12.718	3.127	0.232	125-250
24-25	13.687	3.175	0.235	125-250
28-29	14.239	3.22	0.201	125-250
32-33	14.542	3.378	0.126	125-250
36-37	14.844	3.657	0.103	125-250
40-41	15.344	3.748	0.173	>400
44-45	15.721	3.962	0.015	125-250
48-49	16.108	4.015	0.028	125-250
52-53	16.743	3.928	0.025	125-250
56-57	17.659	3.910	0.035	125-250
60-61	18.574	3.796	0.073	125-250
64-65	19.490	3.901	0.088	125-250
68-69	20.405	3.765	0.072	125-250
72-73	21.321	3.732	0.014	125-250
76-77	22.100	3.751	0.127	125-250
80-81	22.878	3.725	0.162	315-400
84-85	23.657	3.814	-0.052	315-400
88-89	24.435	3.847	0.178	125-250

(B)

Depth (cm)	Age (ka BP)	SiO2 (Gew%)
0-1	6.493	12
3-4	7.386	10
7-8	8.816	10
10-11	9.888	7
11-12	10.245	7
15-17	11.386	6
19-20	12.355	8
20-21	12.597	10
23-24	13.324	9
27-28	14.126	8
30-31	14.353	18
31-32	14.428	11
35-36	14.731	6
39-40	15.168	6
40-41	15.297	7
43-44	15.579	4
47-48	15.956	4
50-51	16.283	4
51-52	16.400	5
55-56	17.316	7
59-60	18.231	4
60-61	18.460	6
63-64	19.147	6
67-68	20.062	5
70-71	20.749	7
71-72	20.978	6
75-76	21.808	6
79-80	22.586	6
80-81	22.781	7
83-84	23.365	4
87-88	24.143	4

(C)

Depth (cm)	Age (ka BP)	Opal MAR (g/(cm2*ka))
0-1	6.493	24
10-11	9.888	17
20-21	12.597	29
30-31	14.353	96
40-41	15.297	55
50-51	16.283	27
60-61	18.460	16
70-71	20.749	20
80-81	22.781	28

Table S5. (continued).

(D)

Depth	Age	XRF		
(cm)	(ka BP)	Fe (cps)	Ca (cps)	Si/Ti (cps/cps)
1	6.672	104731	149744	1.98
2	7.029	107781	160505	2.25
3	7.386	107482	179962	2.45
4	7.744	104935	176828	2.31
5	8.101	106917	179897	2.43
6	8.458	105477	175967	2.32
7	8.816	104681	182799	2.34
8	9.173	98047	196291	2.18
9	9.530	97919	210582	2.18
10	9.888	100662	217745	2.12
11	10.245	103885	246838	2.18
12	10.602	102377	252492	2.05
13	10.902	107716	232884	1.90
14	11.144	82325	343187	2.73
15	11.386	97089	320880	2.59
16	11.629	71635	387743	3.29
17	11.871	72541	357148	3.09
18	12.113	63956	374529	3.23
19	12.355	68222	356364	3.35
20	12.597	66090	346450	3.29
21	12.839	59680	343759	3.62
22	13.081	69718	305852	3.01
23	13.324	62497	315354	3.50
24	13.566	58495	293276	3.48
25	13.808	56738	231679	3.71
26	14.050	60406	227146	3.53
27	14.126	62807	248132	3.78
28	14.201	66717	241181	4.27
29	14.277	68098	236726	4.40
30	14.353	66648	225043	4.63
31	14.428	63177	208682	4.32
32	14.504	67946	236835	4.01
33	14.580	69595	233724	4.18
34	*14.655*	75936	201380	4.16
35	14.731	72998	215420	3.65
36	14.807	76566	211101	3.40
37	14.882	103203	165404	3.04
38	15.003	112819	157739	3.02
39	15.168	102409	181839	3.17
40	15.297	103859	180319	3.06
41	15.391	105162	180983	3.12
42	15.485	119696	148001	3.00
43	15.579	119816	93156	2.73
44	15.674	140755	84299	2.52
45	15.768	133905	92525	2.65
46	15.862	144245	81589	2.56
47	15.956	154566	69765	2.43
48	16.050	158619	52041	2.31
49	16.167	152824	48904	2.39
50	16.283	151868	54213	2.50
51	16.400	149985	54060	2.36
52	16.629	155679	50490	2.28
53	16.858	171213	68159	2.45
54	17.087	154331	84726	2.64
55	17.316	130295	117858	2.94
56	17.544	123394	129278	3.06
57	17.773	124008	135124	3.19
58	18.002	121637	144686	3.04
59	18.231	114262	171946	3.17
60	18.460	116713	156529	3.17
61	18.689	127889	135680	3.06
62	18.918	127186	150658	3.08
63	19.147	114478	154913	3.12
64	19.375	118410	140561	2.99
65	19.604	115297	139094	2.88
66	19.833	124342	123026	2.76
67	20.062	126747	119028	2.97
68	20.291	124397	117498	2.93
69	20.520	128784	112986	2.82
70	20.749	127896	100113	2.71
71	20.978	129637	85915	2.47
72	21.207	108213	61259	2.25
73	21.418	118033	79309	2.67
74	21.613	125646	116630	2.86
75	21.808	127287	95137	2.60
76	22.002	122967	104003	2.58
77	22.197	125011	115549	2.70
78	22.391	117437	118272	2.88
79	22.586	109135	114328	2.90

References Supporting Information

Bevington, P. R., and D. K. Robinson (2003), Data Reduction and Error Analysis for Physical Sciences, 3rd edition, McGraw-Hill, New York.

Chapligin, B., H. Meyer, H. Friedrichsen, A. Marent, E. Sohns, and H.-W. Hubberten (2010), A high-performance, safer and semi-automated approach for the $\delta^{18}O$ analysis of diatom silica and new methods for removing exchangeable oxygen, *Rapid Communications in Mass Spectrometry*, *24*, 2655-2664.

De la Rocha, C. L., M. A. Brzezinski, and M. J. DeNiro (1997), Fractionation of silicon isotopes by marine diatoms during biogenic silica formation, *Geochimica et Cosmochimica Acta*, *61*, 5051-5056.

Galbraith, E. D., S. L. Jaccard, T. F. Pedersen, D. M. Sigman, G. H. Haug, M. Cook, J. R. Southon, and R. Francois (2007), Carbon dioxide release from the North Pacific abyss during the last deglaciation, *Nature*, *449*, 890-894.

Gebhardt, H., M. Sarnthein, P. M. Grootes, T. Kiefer, H. Kuehn, F. Schmieder, and U. Röhl (2008), Paleonutrient and productivity records from the subarctic North Pacific for Pleistocene glacial terminations I to V, *Paleoceanography*, *23*, PA4212.

Keigwin, L. D. (1987), North Pacific deep water formation during the last glaciation, *Nature*, *330*, 362-364.

Keigwin, L. D., G. A. Jones, and P. N. Froelich (1992), A 15,000 year paleoenvironmental record from Meiji Seamount, far northwestern Pacific, *Earth and Planetary Science Letters*, *111*, 425-440.

Kienast S.S., and J. L. McKay (2001), Sea Surface Temperatures in the subarctic Northeast Pacific reflect millennial-scale Climate Oscillations during the last 16 kyrs, *Geophysical Research Letters*, *28*, 1563-1566.

Kovanen, D. J., and D. J. Easterbrook (2002), Paleodeviations of radiocarbon marine reservoir values for the northeast Pacific, *Geology*, *30*, 243-246.

Juillet-Leclerc, A., and L. Labeyrie (1987), Temperature dependance of the oxygen isotopic fractionation between diatom silica and water, *Earth and Planetary Science Letters*, *84*, 69-74.

Lopes, C., and A. C. Mix (2009), Pleistocene megafloods in the northeast Pacific, *Geology*, *37*, 79-82.

Lund, D. C., A. C. Mix, and J. Southon (2011), Increased ventilation age of the deep northeast Pacific Ocean during the last deglaciation, *Nature Geoscience*, *4*, 771-774.

Maier, E., B. Chapligin, A. Abelmann, R. Gersonde, O. Esper, J. Ren, H. Friedrichsen, H. Meyer, and R. Tiedemann (2013), Combined oxygen and silicon isotope analysis of diatom silica from a deglacial subarctic Pacific record, *Journal of Quaternary Science*, *28*, 571-581.

Milligan, A. J., D. E. Varela, M. A. Brzezinski, and F. M. M. Morel (2004), Dynamics of silicon metabolism and silicon isotopic discrimination in a marine diatom as a function of $p\mathrm{CO_2}$, *Limnology and Oceanography*, *49*, 322-329.

Reimer, P. J., E. Bard, A. Bayliss, J. W. Beck, P. G. Blackwell, C. Bronk Ramsey, C. E. Buck, H. Cheng, R. L. Lawrence, M. Friedrich, P. M. Grootes, T. P. Guilderson, H. Haflidason, I. Hajdas, C. Hatté, T. J.

Heaton, D. L. Hoffman, A. G. Hogg, K. A. Hughen, K. F. Kaiser, B. Kromer, S. W. Manning, M. Niu, R. W. Reimer, D. A. Richards, E. M. Scott, J. R. Southon, R. A. Staff, C. S. M. Turney, and J. van der Pflicht (2013), INTCAL13 and MARINE13 radiocarbon age calibration curves 0-50,000 years cal BP, *Radiocarbon*, *55*, 1869-1887.

Sabin, A. L., and N. G. Pisias (1996), Sea Surface Temperature Changes in the Northeastern Pacific Ocean during the Past 20,000 Years and Their Relationship to Climate Change in Northwestern North America, *Quaternary Research*, *46*, 48-61.

Sarnthein, M., S. Balmer, P. M. Grootes and M. Muddelsee (2015), Planktic and benthic ^{14}C reservoir ages for three ocean basins calibrated by a suite of ^{14}C plateaus in the glacial-to-deglacial Suigetsu atmospheric ^{14}C record, *Radiocarbon*, *57*, 129-151.

Sarnthein, M., P. M. Grootes, J. P. Kennett, and M.-J. Nadeau (2007), ^{14}C Reservoir Ages Show Deglacial Changes in Ocean Currents and Carbon Cycle, *Geophysical Monograph Series*, *173*, 175-196.

Sarnthein, M., H. Gebhardt, T. Kiefer, M. Kucera, M. Cook, and H. Erlenkeuser (2004), Mid Holocene origin of the sea-surface salinity low in the subarctic North Pacific, *Quaternary Science Reviews*, *23*, 2089-2099.

Stuiver, M., and P. J. Reimer (1993), Extended ^{14}C data base and revised CALIB 3.0 ^{14}C age calibration program, *Radiocarbon*, *35*, 215-230.

Sun, X., M. Olofsson, P.S. Andersson, B. Fry, C. Legrand, C. Humborg and C.-M. Mörth (2014), Effects of growth and dissolution on the fractionation of silicon isotopes by estuarine diatoms, *Geochimica et Cosmochimica Acta*, *130*, 156-166.

Sutton, J. N., D. E. Varela, M. A. Brzezinski, C. P. Beucher (2013), Species-dependent silicon isotope fractionation by marine diatoms, *Geochimica et Cosmochimica Acta, 104*, 300-309.

Waelbroeck, C., L. Labeyrie, E. Michel, J. C. Duplessy, J. F. McManus, K. Lambeck, E. Balbon, and M. Labracherie (2002), Sea-level and deep water temperature changes derived from benthic foraminifera isotopic records, *Quaternary Science Reviews*, *21*, 295-305.